

SuperiorGAT: Graph Attention Networks for Sparse LiDAR Point Cloud Reconstruction in Autonomous Systems

Khalfalla Awedat^{1,*}, Mohamed Abidalrekab², Gurcan Comert³, and Mustafa Ayad⁴

¹Computer Information Technology Department, SUNY Morrisville College, Morrisville, NY, USA

²Electrical and Computer Engineering, Portland State University, Portland, OR, USA

³Computational Data Science and Engineering Department, North Carolina A&T State University, Greensboro, NC, USA

⁴Electrical and Computer Engineering Department, SUNY Oswego, Oswego, NY, USA

*awedatk@morrisville.edu

ABSTRACT

LiDAR-based perception in autonomous systems is constrained by fixed vertical beam resolution and further compromised by beam dropout resulting from environmental occlusions. This paper introduces **SuperiorGAT**, a graph attention-based framework designed to reconstruct missing elevation information in sparse LiDAR point clouds. By modeling LiDAR scans as beam-aware graphs and incorporating gated residual fusion with feed-forward refinement, SuperiorGAT enables accurate reconstruction without increasing network depth. To evaluate performance, structured beam dropout is simulated by removing every fourth vertical scanning beam. Extensive experiments across diverse KITTI environments, including **Person**, **Road**, **Campus**, and **City** sequences, demonstrate that SuperiorGAT consistently achieves lower reconstruction error and improved geometric consistency compared to PointNet-based models and deeper GAT baselines. Qualitative X-Z projections further confirm the model's ability to preserve structural integrity with minimal vertical distortion. These results suggest that architectural refinement offers a computationally efficient method for improving LiDAR resolution without requiring additional sensor hardware providing a foundation for real-time optimization on embedded hardware.

Introduction

Autonomous vehicles rely critically on Light Detection and Ranging (LiDAR) sensors for 3D environmental perception, enabling precise object detection, localization, and mapping essential for safe navigation^{1,2}. Despite their fundamental importance, LiDAR systems face a critical vulnerability: performance severely degrades under structured data loss, particularly beam dropout caused by hardware malfunctions or environmental occlusions, which disrupts spatial continuity and compromises downstream tasks such as object detection and path planning^{1,3}. This challenge is particularly acute for cost-effective LiDAR systems that employ fewer scanning beams (typically 16-32 beams compared to 64+ in premium systems), inherently producing sparse point clouds that demand robust reconstruction methods to achieve the high-resolution performance required for autonomous operation⁴.

Current reconstruction approaches face a fundamental trade-off between accuracy and computational efficiency, limiting their practical deployment. Compressive sensing (CS) methods provide theoretical guarantees for sparse signal recovery but depend on computationally intensive iterative solvers that render them impractical for the real-time constraints of autonomous systems^{5,6}. Convolutional neural networks (CNNs), particularly voxel-based architectures, demonstrate effectiveness in processing point clouds but necessitate dense 3D projections, resulting in inefficient memory usage and computational overhead when applied to inherently sparse LiDAR data^{7,8}.

Recent advances in deep learning, including hierarchical point cloud models that operate directly on unordered point sets, have shown promise but remain inadequate for addressing the structured sparsity patterns characteristic of beam dropout scenarios⁹. While Graph Neural Networks (GNNs), especially Graph Attention Networks (GATs), have demonstrated significant potential in modeling complex geometric relationships within irregular data structures through sophisticated graph representations¹⁰⁻¹², standard graph-based approaches, including graph convolutional networks, often fail to effectively prioritize the critical local geometric features essential for high-fidelity reconstruction of sparse LiDAR data¹³. Our recent conference work demonstrated that multi-layer Graph Attention Networks can effectively reconstruct missing LiDAR elevation values using raw point-cloud geometry alone, without relying on RGB images or temporal information¹⁴. While increasing network depth improved reconstruction fidelity, deeper attention stacks introduced higher computational cost and stability

limitations. In this work, which extends our previous findings, we move beyond depth-based improvements and focus on architectural refinement to achieve superior performance with a lightweight, single-layer design incorporating gated residual fusion.

To address these fundamental limitations, we propose SuperiorGAT, a novel graph attention-based framework specifically engineered to reconstruct sparse LiDAR point clouds with exceptional fidelity while maintaining the computational efficiency necessary for real-time deployment in autonomous systems^{8,12}. Our approach directly tackles the structured sparsity challenge through several key innovations. SuperiorGAT implements a realistic beam dropout simulation framework that accurately mimics hardware faults observed in real-world LiDAR deployments, providing a robust testing environment for autonomous vehicle applications^{1,3}. The system constructs optimized k-nearest neighbor graphs to effectively represent sparse point cloud structures while incorporating specialized beam index features that enhance both spatial and structural contextual understanding¹².

The model architecture features a carefully designed, lightweight framework that incorporates multiple graph attention layers with multi-head attention mechanisms and residual connections, enabling highly efficient processing of sparse data without the computational burden of iterative CS optimization or the memory overhead of dense CNN projections¹¹. By directly addressing structured sparsity patterns, SuperiorGAT provides a scalable and practical solution for autonomous driving applications, successfully bridging the critical gap between high-resolution reconstruction accuracy and real-time computational efficiency. Our primary contributions to the field include:

1. A comprehensive and realistic simulation framework for structured beam dropout that accurately reflects hardware faults and environmental conditions encountered in real-world LiDAR systems.
2. A novel graph attention-based reconstruction architecture that dynamically optimizes point-to-point interactions through learned attention weights, effectively preserving fine-grained structural details essential for autonomous navigation.
3. A computationally efficient framework specifically designed for real-time deployment constraints, offering significant potential for practical integration in autonomous vehicle systems.

The remainder of this paper is structured as follows. Section 2 provides a comprehensive review of related work in LiDAR point cloud reconstruction and graph-based methodologies. Section 3 presents detailed technical specifications of the SuperiorGAT methodology, including data preprocessing pipelines and architectural design principles. Section 4 describes our experimental framework and evaluation protocols, followed by a comprehensive analysis of the results and performance in Section 5. Section 6 discusses the broader implications of our findings, practical limitations, and potential applications, while Section 7 concludes with future research directions and development paths.

Related Work

Light Detection and Ranging (LiDAR) technology is a cornerstone of 3D perception for autonomous vehicles, enabling tasks like object detection and mapping through precise geometric data^{2,3}. Yet, sparse point clouds—caused by low-resolution sensors or beam dropout from environmental factors such as rain or hardware faults—complicate accurate reconstruction². As illustrated in Figure 1, beam dropout predominantly disrupts elevation (z-coordinates), while x and y coordinates, derived from azimuthal scans, remain stable, underscoring the need for targeted z-reconstruction methods^{15,16}. This vertical sparsity arises from the limited number of laser channels in affordable LiDAR systems, a challenge evident in datasets such as KITTI².

Conventional reconstruction techniques include interpolation and compressive sensing (CS). Interpolation methods, such as linear or nearest-neighbor approaches, estimate missing points based on proximity but often smooth out critical geometric features, particularly in complex scenes^{5,6,17}. Advanced techniques, such as spline interpolation, reduce this issue but can introduce artifacts in regions with sharp elevation shifts¹⁷. CS offers a theoretical framework for recovering sparse signals but demands computationally intensive iterative processes, rendering it unsuitable for real-time applications where sub-100 millisecond (ms) inference is critical^{5,6,11}. These limitations underscore the need for efficient solutions specifically designed for LiDAR's structured sparsity.

Deep learning has transformed point cloud processing, with Convolutional Neural Networks (CNNs) like VoxelNet converting sparse data into dense voxel grids for tasks such as 3D object detection⁷. However, this densification escalates computational costs and erodes fine details in sparse LiDAR data^{7,18}. VoxelNet's cubic scaling with resolution contrasts with PointNet++, which employs hierarchical sampling to handle irregular data; yet, both methods falter with structured dropout patterns due to static feature aggregation^{9,19}. PointNet and its extensions leverage permutation invariance but struggle to adapt to the specific sparsity of beam dropout^{9,15}.

Recent advances in LiDAR super-resolution target vertical resolution enhancement, focusing on z-coordinates for improved pedestrian detection^{15,18}. You and Kim (2023) introduced a 2D range image-based upsampling technique, interpolating x, y, z,

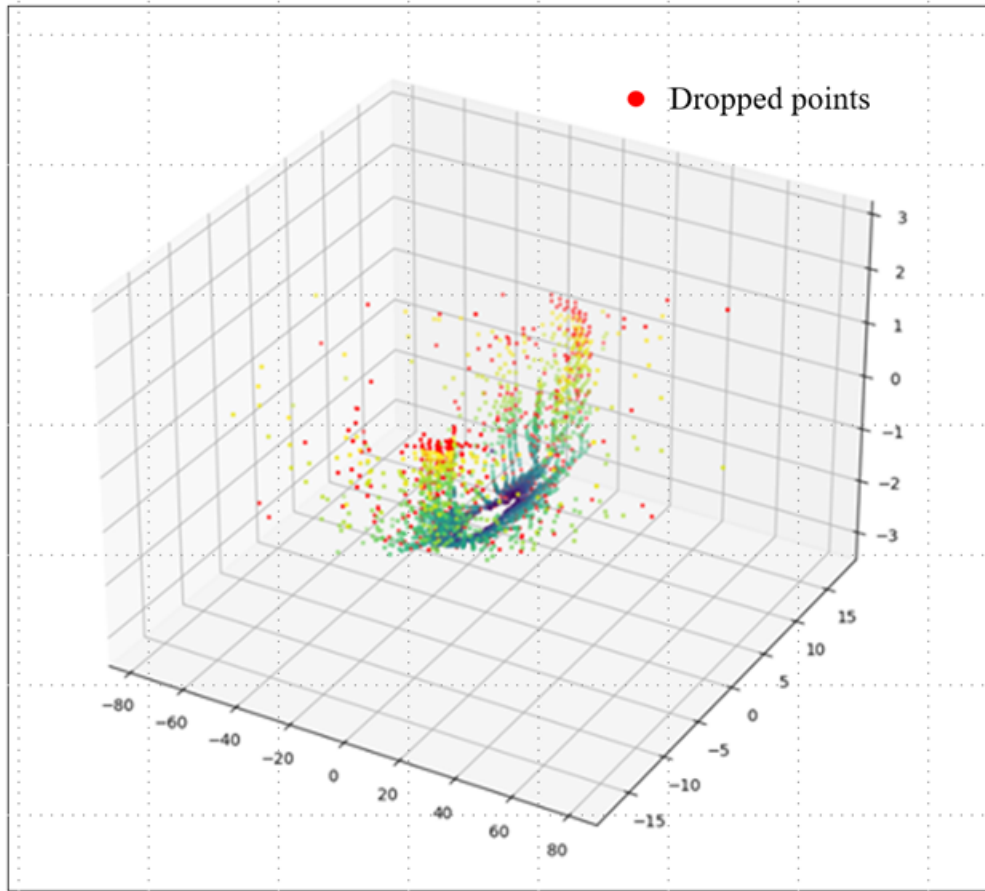


Figure 1. LiDAR point cloud with beam dropout (KITTI Residential dataset). Original 64-beam point cloud (colored by z-coordinate) with 25% beam dropout points in red, simulating missing z-coordinates due to hardware or environmental faults. SuperiorGAT reconstructs these z-values for autonomous driving.

and intensity to boost 3D detection accuracy, while Eskandar et al. (2023) proposed HALS, a height-aware model using polar coordinate regression to excel on KITTI data^{15,18}. These approaches affirm z-reconstruction’s importance, given the reliability of x and y coordinates in LiDAR scans², though their reliance on dense architectures limits real-time viability.

Graph Neural Networks (GNNs) provide a versatile framework for modeling irregular data, where points are represented as nodes and relationships are represented as edges¹⁰. Graph Convolutional Networks (GCNs) employ fixed-weight convolutions, which are effective for node classification but less adept at prioritizing sparse LiDAR geometries¹³. Enhanced GNNs incorporate edge attributes, such as distances, thereby enhancing spatial modeling^{12,20}. Graph Attention Networks (GATs), pioneered by Veličković et al., introduce dynamic weighting via attention mechanisms, drawing from insights from neural machine translation^{11,21}. Although successful in network analysis, GATs remain underexplored for LiDAR, where their adaptive aggregation is particularly suited to sparse geometries²⁰.

Recent work in graph neural networks has explored architectural elements that enhance stability and expressive capacity beyond the standard GAT formulation. In particular, gated skip connections have been shown to improve gradient flow and help models balance raw node features with attention-refined representations^{22,23}. Building upon our prior work¹⁴, which established the effectiveness of multi-layer GAT architectures for recovering missing elevation data, this research extends that foundation by introducing a more efficient architectural design. By incorporating gated residual fusion and feed-forward refinement, we achieve improved reconstruction accuracy while eliminating the need for increasing graph depth.. Likewise, several graph transformer variants incorporate feed-forward sublayers similar to those used in sequence transformers to increase nonlinear capacity and improve local geometric modeling²⁴. These ideas motivate our adoption of a lightweight gated residual pathway and a transformer-style feed-forward block, adapted specifically to the characteristics of sparse LiDAR reconstruction.

SuperiorGAT advances GATs by optimizing for LiDAR z-reconstruction, integrating beam index features to reflect scanning patterns, and employing a lightweight design with multi-head attention and residuals^{11,20}. Unlike previous methods, it tackles

structured beam dropout (Figure 1) with a focus on z-coordinates, offering a balance of accuracy and efficiency for autonomous driving. This sets it apart from dense CNN approaches⁷, PointNet variants⁹, and super-resolution techniques^{15,18}, establishing a novel real-time solution.

Graph-Based Reconstruction Methodology

Graph Neural Networks (GNNs)

Graph Neural Networks (GNNs) represent a powerful class of deep learning models designed to perform inference on data described by graphs. By leveraging the inherent relational structure of graph data, GNNs overcome a key limitation of traditional neural networks, which require input data to exist in an independent and identically distributed (i.i.d.) or grid-like structure (e.g., images)^{10,25}.

The core operational principle of GNNs is *message passing*, a framework where nodes in a graph iteratively aggregate information from their local neighbors to build increasingly sophisticated representations of themselves and their context^{25,26}. This process can be broken down into three steps at each layer l :

- **Message ($m_{ij}^{(l)}$):** For every edge connecting node j to node i , a message is computed as a function of the features of the sender node j , the receiver node i , and the edge features e_{ij} :

$$m_{ij}^{(l)} = \phi^{(l)}(h_i^{(l)}, h_j^{(l)}, e_{ij}) \quad (1)$$

- **Aggregation ($a_i^{(l)}$):** Node i collects messages from its neighbors $\mathcal{N}(i)$ and combines them using a permutation-invariant aggregation function (e.g., sum, mean, max):

$$a_i^{(l)} = \bigoplus_{j \in \mathcal{N}(i)} m_{ij}^{(l)} \quad (2)$$

- **Update ($h_i^{(l+1)}$):** The node updates its representation by combining its previous features with the aggregated neighborhood message:

$$h_i^{(l+1)} = \psi^{(l)}(h_i^{(l)}, a_i^{(l)}) \quad (3)$$

This mechanism is illustrated in Fig. 2, which depicts a two-layer GNN where the central node iteratively aggregates information from its neighbors and their neighbors.

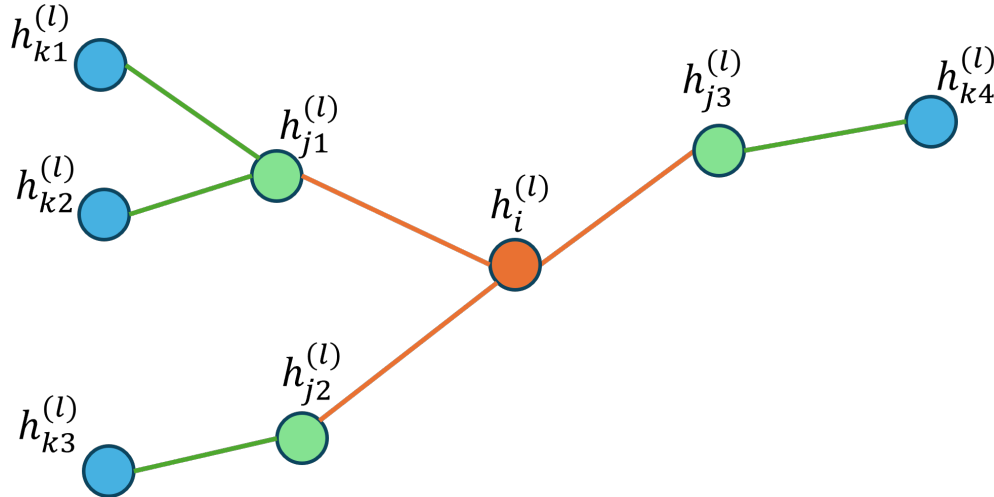


Figure 2. Illustration of two-layer message passing in a GNN.

This mechanism allows each node to progressively incorporate information from multi-hop neighborhoods. For example, in a 2-layer GNN, a central node aggregates features from its direct neighbors in the first layer, and from its neighbors' neighbors in the second layer. This ability to capture higher-order structural dependencies makes GNNs particularly effective for tasks where node states are influenced by spatial and relational context^{2,13,27}.

Problem Formulation

Light Detection and Ranging (LiDAR) systems generate point clouds as unordered sets of points $\mathcal{P} = \{p_i\}$, where each $p_i = (x_i, y_i, z_i, r_i)$ includes 3D coordinates and reflectance intensity. These systems are prone to beam dropout, modeled by a function $\mathcal{D}(\cdot)$, which removes points from specific beams due to hardware limitations or environmental factors, resulting in a sparse subset $\mathcal{P}_{\text{sparse}} \subset \mathcal{P}$. This dropout particularly affects z-coordinates, critical for spatial perception in applications like autonomous navigation. The objective is to learn a mapping function f_θ that reconstructs the missing z-values: $\hat{z}_i = f_\theta(\mathcal{P}_{\text{sparse}})$, restoring elevation data while assuming x and y coordinates remain reliable. As illustrated in Figure 1, this targeted reconstruction addresses a common challenge in sparse LiDAR data.

Graph Representation

To formulate this as a graph problem, we represent $\mathcal{P}_{\text{sparse}}$ as a graph $\mathcal{G} = (\mathcal{V}, \mathcal{E})$. Nodes \mathcal{V} correspond to points p_i , with feature vectors $\mathbf{v}_i = [x_i, y_i, \tilde{z}_i, b_i]$, where \tilde{z}_i is the observed z-coordinate (or 0 if dropped) and b_i is a beam index reflecting the sensor's vertical structure. Edges \mathcal{E} are defined to capture the LiDAR's scan pattern, connecting points within the same beam sequentially to form intra-beam relationships, and linking points across adjacent beams to model surface continuity. This approach prioritizes the sensor's inherent geometry over pure spatial proximity, offering a flexible representation suitable for graph-based methods.

Preparation for GNN Application

This graph structure enables the application of Graph Neural Networks (GNNs) to model local relationships among points, leveraging the beam-aware connectivity to infer missing z-values. The representation provides a foundation for advanced graph-based techniques, setting the stage for exploring convolutional and attention-based approaches to enhance reconstruction accuracy. This prepares the framework for the subsequent development of tailored GNN architectures.

GNN Architectures for LiDAR Reconstruction

Graph Convolutional Networks (GCN) as Baseline

We begin with Graph Convolutional Networks (GCNs) as a baseline approach to process the graph representation of LiDAR data. GCNs aggregate features from neighboring nodes using fixed weights based on the graph structure, enabling the model to learn spatial patterns for z-reconstruction. This method applies convolutional operations over the graph, leveraging the beam-aware edges to propagate information. While effective for initial feature extraction, GCNs' uniform weighting limits their ability to prioritize critical local features, motivating the need for a more adaptive approach.

Graph Attention Networks: Theoretical Foundation

Graph Attention Networks (GATs) represent a significant advancement in graph representation learning by introducing an attention mechanism that enables dynamic, content-aware neighborhood aggregation¹¹. Unlike Graph Convolutional Networks (GCNs) that employ fixed-weight aggregation based on graph structure, GATs compute adaptive attention coefficients that weight the contribution of each neighbor during feature propagation, allowing the model to focus on the most relevant contextual information for sparse LiDAR reconstruction.

The core innovation lies in the self-attention mechanism that operates on node pairs. For a given node i with features \mathbf{h}_i and its neighbor $j \in \mathcal{N}(i)$, the attention mechanism first applies a shared linear transformation parameterized by weight matrix $\mathbf{W} \in \mathbb{R}^{F' \times F}$:

$$\mathbf{h}'_i = \mathbf{W}\mathbf{h}_i, \quad \mathbf{h}'_j = \mathbf{W}\mathbf{h}_j \quad (4)$$

The unnormalized attention coefficient is then computed as:

$$e_{ij} = \text{LeakyReLU}(\mathbf{a}^T [\mathbf{h}'_i \parallel \mathbf{h}'_j]) \quad (5)$$

where $\mathbf{a} \in \mathbb{R}^{2F'}$ is a learnable attention vector, and \parallel denotes vector concatenation. The attention coefficients are normalized across the neighborhood using the softmax function:

$$\alpha_{ij} = \frac{e^{(e_{ij})}}{\sum_{k \in \mathcal{N}(i)} e^{(e_{ik})}} \quad (6)$$

The updated node representation is computed as the attention-weighted aggregation:

$$\mathbf{h}_i^{\text{out}} = \sigma \left(\sum_{j \in \mathcal{N}(i)} \alpha_{ij} \mathbf{h}'_j \right) \quad (7)$$

where σ is a nonlinear activation function. This formulation enables anisotropic aggregation, where each neighbor’s contribution is dynamically weighted based on feature compatibility, providing a more expressive scheme than isotropic approaches^{11,26}. The standard GAT architecture follows the sequential processing pipeline illustrated in Figure 3a.

SuperiorGAT: Enhanced Architecture for LiDAR Reconstruction

The core of our proposed framework is the SuperiorGAT layer, which is designed to capture complex local geometries without the computational burden of deep network stacks. While standard GATs as depicted in Figure 3(a) provide adaptive neighbor weighting, they lack several components crucial for handling the distinctive sparsity patterns and irregular geometry of LiDAR point clouds. Our preliminary testing and previous research¹⁴ demonstrated that a single standard layer lacks the representational capacity required for high-fidelity LiDAR reconstruction. Consequently, our earlier work¹⁴ relied on stacking multiple GAT layers to achieve competitive results. To address these limitations, we propose SuperiorGAT a specialized architecture with targeted enhancements for reconstructing missing points in sparse 3D scans. The overall framework comparison is illustrated in Figure 3(b), while the detailed computational pipeline is shown in Figure 4. By incorporating a gated residual connection, the model can preserve the original spatial coordinates (identity) while selectively integrating features learned through the attention mechanism. This approach allows SuperiorGAT to outperform multi-layer baselines using only a single refined layer, providing a more efficient solution for spatial data recovery.

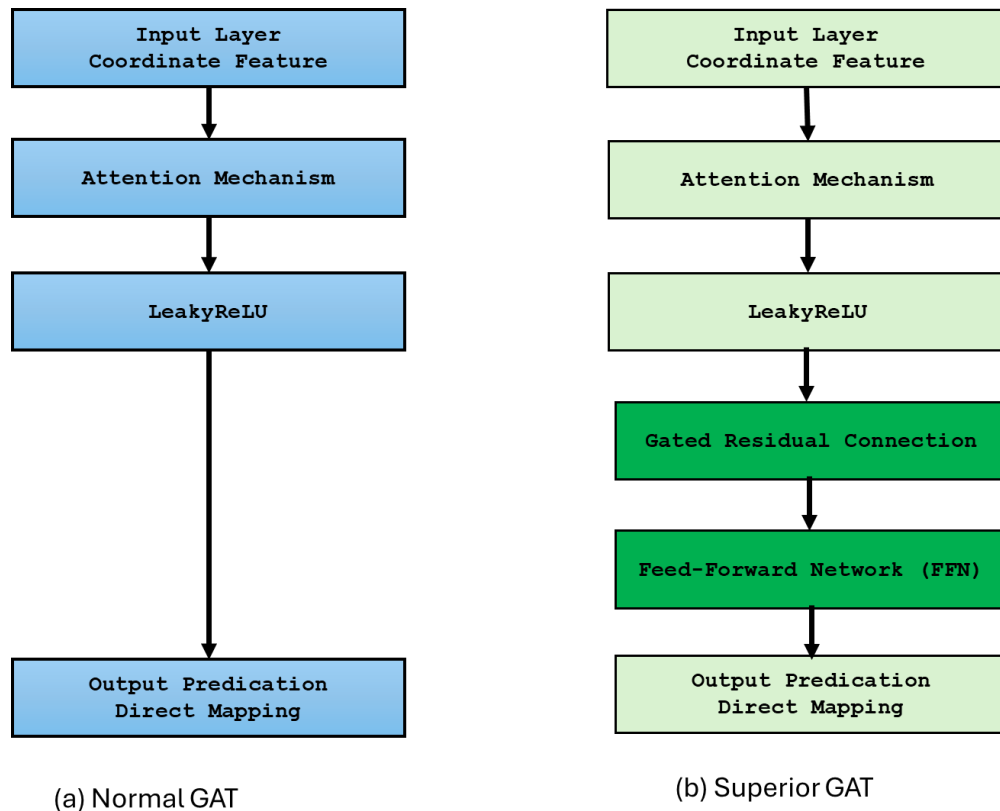


Figure 3. GAT architecture comparison. (a) Standard implementation. (b) SuperiorGAT with domain-specific enhancements for LiDAR reconstruction.

As visualized in Figure 4, SuperiorGAT processes each node through four sequential stages: (1) beam-aware feature encoding, (2) multi-head attention aggregation, (3) gated residual fusion, and (4) feed-forward refinement with task-specific decoding.

Beam-Aware Feature Encoding. SuperiorGAT begins by enriching each node with structural information from the LiDAR sensor configuration. Rather than relying solely on spatial coordinates, each point i is represented with scan-pattern context:

$$\mathbf{h}_i^{(0)} = [x_i, y_i, \tilde{z}_i, b_i], \quad (8)$$

where b_i denotes the beam index. This encoding provides critical geometric context about the LiDAR scanning mechanism and significantly enhances the model’s capacity to reason about missing depths resulting from beam dropout.

Multi-Head Attention with Adaptive Aggregation. The encoded features undergo multi-head graph attention to capture diverse geometric relationships. For each attention head k , the node representation is updated as:

$$\mathbf{h}_i^{\text{attn},k} = \sigma \left(\sum_{j \in \mathcal{N}(i)} \alpha_{ij}^k \mathbf{W}^k \mathbf{h}_j^{(0)} \right), \quad (9)$$

where α_{ij}^k are the attention coefficients from head k , \mathbf{W}^k is the head-specific weight matrix, and σ denotes the activation function. The outputs from all K heads are concatenated:

$$\mathbf{h}_i^{\text{attn}} = \left\| \left\|_{k=1}^K \mathbf{h}_i^{\text{attn},k} \right. \right. \quad (10)$$

where $\mathbf{h}_i^{\text{attn},k} \in \mathbb{R}^{F'}$ is the output of head k , so that $\mathbf{h}_i^{\text{attn}} \in \mathbb{R}^{KF'}$ collects all heads into a single feature vector.

Stabilized Attention Through Residual Gating. Following attention aggregation, SuperiorGAT employs a gated residual mechanism that dynamically balances the attention-refined features with the original normalized input:

$$\mathbf{h}_i^{\text{gated}} = \text{LayerNorm}(\gamma \cdot \mathbf{h}_i^{\text{attn}} + (1 - \gamma) \cdot \mathbf{h}_i^{\text{norm}}), \quad (11)$$

where $\gamma \in [0, 1]$ is a learnable gate parameter and $\mathbf{h}_i^{\text{norm}}$ represents the normalized input features. This adaptive gating mechanism provides crucial stability in regions where neighborhood information may be unreliable due to sparse sampling or beam dropout.

Feed-Forward Refinement. The gated representations then pass through a compact feed-forward network (FFN) for non-linear feature enhancement. A residual connection preserves structural information throughout this refinement:

$$\mathbf{h}_i^{\text{final}} = \text{LayerNorm}(\text{FFN}(\mathbf{h}_i^{\text{gated}}) + \mathbf{h}_i^{\text{gated}}), \quad (12)$$

where $\text{FFN}(\mathbf{x}) = \mathbf{W}_2 \cdot \text{LeakyReLU}(\mathbf{W}_1 \mathbf{x} + \mathbf{b}_1) + \mathbf{b}_2$. This expansion-contraction design enhances representational capacity without significantly increasing computational complexity.

Task-Specific Output Decoding. The final refined feature vector $\mathbf{h}_i^{\text{final}}$ is processed by a lightweight multi-layer perceptron optimized specifically for elevation recovery:

$$\hat{z}_i = \text{MLP}_{\text{decoder}}(\mathbf{h}_i^{\text{final}}). \quad (13)$$

This regression-focused output head predicts the reconstructed depth value \hat{z}_i for each point, completing the restoration of missing elevation data.

The integrated combination of beam-index encoding, multi-head attention with adaptive aggregation, gated residual stabilization, FFN refinement, and specialized decoding enables SuperiorGAT to effectively address the distinctive challenges of LiDAR point cloud reconstruction under beam dropout conditions. As illustrated in Figure 4, SuperiorGAT uses two distinct residual pathways: one before the gated fusion and another inside the FFN block, ensuring stable propagation of geometric information.

Experimental Setup and Evaluation

Experimental Setup

All experiments were conducted using the KITTI raw LiDAR dataset²⁸, focusing on a residential driving sequence recorded with a Velodyne HDL-64E sensor operating at 10 Hz. The selected sequence contains 107 frames and represents a typical urban residential scenario. Each LiDAR scan provides three-dimensional point coordinates, from which approximately 50,000 points per frame were retained using stratified sampling to preserve the vertical beam structure.

To simulate realistic sensor degradation, structured beam dropout was applied by removing every fourth LiDAR beam, resulting in approximately 25% data loss per frame. This process introduces vertical sparsity that reflects common failure modes in cost-effective or degraded LiDAR systems. The dropout pattern was fixed and applied consistently across frames.

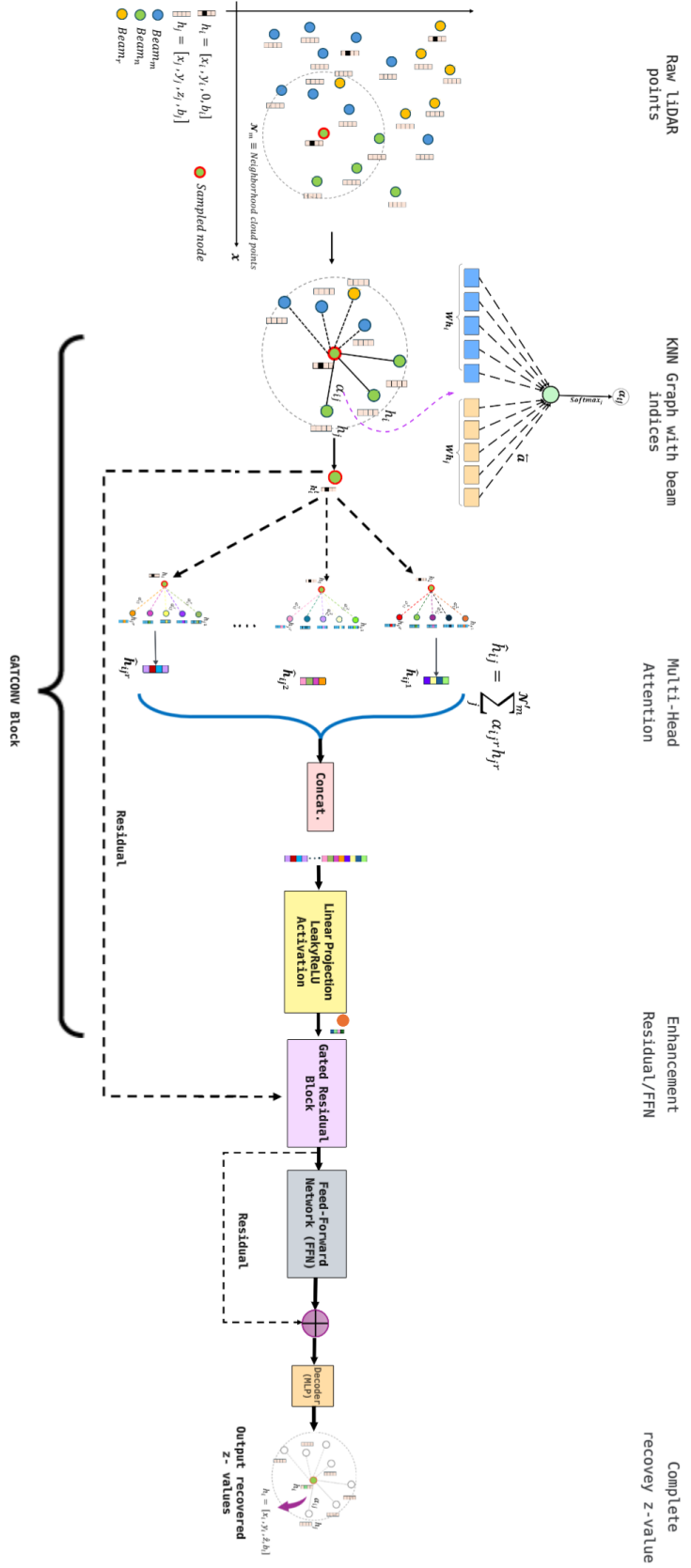


Figure 4. Beam-indexed graph structure used for LiDAR point reconstruction, illustrating intra- and inter-beam connections. Dropped points are marked to show the reconstruction target.

Each sparse point cloud was represented as a graph using a k -nearest neighbor construction, where k denotes the neighborhood size. Node features consisted of the spatial coordinates (x, y) , a masked z -coordinate (set to zero for dropped points), and the corresponding beam index. Graphs were constructed independently for each frame.

To isolate the effectiveness of the architectural refinement, models were trained and evaluated independently per frame. Following the constraints established in our previous work¹⁴, no temporal information, RGB data, or cross-frame learning was utilized in any experiment, ensuring the reconstruction relies purely on geometric graph dependencies within a single sweep.

All models were implemented using PyTorch and PyTorch Geometric. Performance was evaluated exclusively on the dropped points using root mean square error (RMSE) and Chamfer distance, along with per-frame inference time to assess computational efficiency.

Results and Discussion

The performance of the SuperiorGAT model was first evaluated through a sensitivity analysis of the neighborhood parameter k using the residential dataset. This parameter is critical as it defines the local graph connectivity and directly influences the receptive field of the attention mechanism. To identify the optimal balance between reconstruction accuracy and computational efficiency, we varied $k \in \{5, 10, 15, 20\}$, with the results illustrated in Fig. 5.

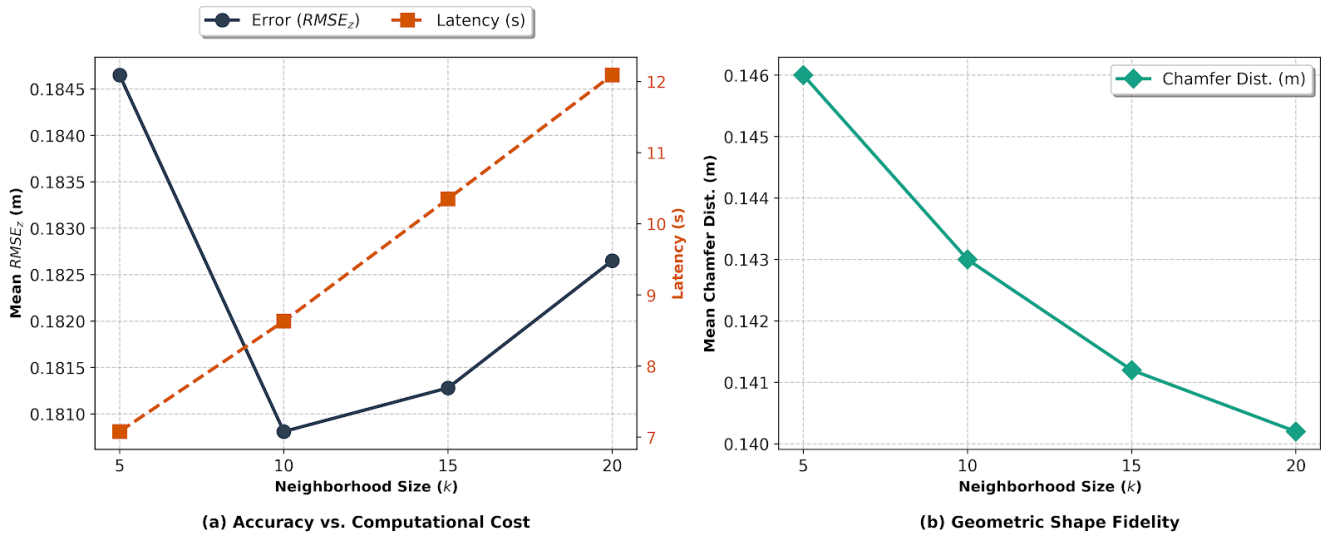


Figure 5. Sensitivity analysis of the neighborhood size k illustrating (a) the relationship between vertical reconstruction error ($RMSE_z$) and inference latency, and (b) the corresponding geometric shape fidelity measured by Chamfer distance.

Our results indicate that $k = 10$ provides the peak performance, achieving the lowest vertical error with an $RMSE_z$ of 0.1808 m. While increasing k beyond this point improves the global geometric shape (as shown by the decreasing Chamfer distance in Fig. 5b), it leads to a slight degradation in vertical precision ($RMSE_z$) due to over-smoothing of local terrain features. Furthermore, $k = 10$ maintains a highly efficient inference latency of 8.63 s, demonstrating a favorable balance between computational demand and reconstruction accuracy. Based on these findings, $k = 10$ was selected as the optimal configuration and is utilized for all subsequent experiments across diverse environments, including the KITTI campus, person, city, and road datasets.

The observed performance trends in Fig. 5 highlight the trade-off between local feature extraction and global context. When k is small ($k = 5$), the graph is too sparse to capture sufficient spatial relationships, leading to higher reconstruction errors. Conversely, at $k = 20$, the inclusion of distant neighbors introduces noise and leads to a "smoothing" effect that obscures fine terrain details, which is reflected in the rising $RMSE_z$. The linear increase in latency from 7.08 s to 12.09 s further confirms that $k = 10$ is the optimal "elbow point" for computational efficiency. Having established $k = 10$ as the optimal hyperparameter, we now evaluate the robustness of SuperiorGAT by comparing it against state-of-the-art baselines across multiple diverse LiDAR environments.

Following the sensitivity analysis, we evaluate the SuperiorGAT model against traditional interpolation techniques and deep learning baselines. This comparison is conducted on the residential dataset using the optimized $k = 10$ configuration. The quantitative results across four key metrics are illustrated in Fig. 6.

The benchmarking results demonstrate that SuperiorGAT achieves superior global reconstruction accuracy. Specifically, it yields the lowest $RMSE_{xyz}$ (0.104 m) and Chamfer distance (0.143 m) among all tested methods. While Nearest Neighbor (NN)

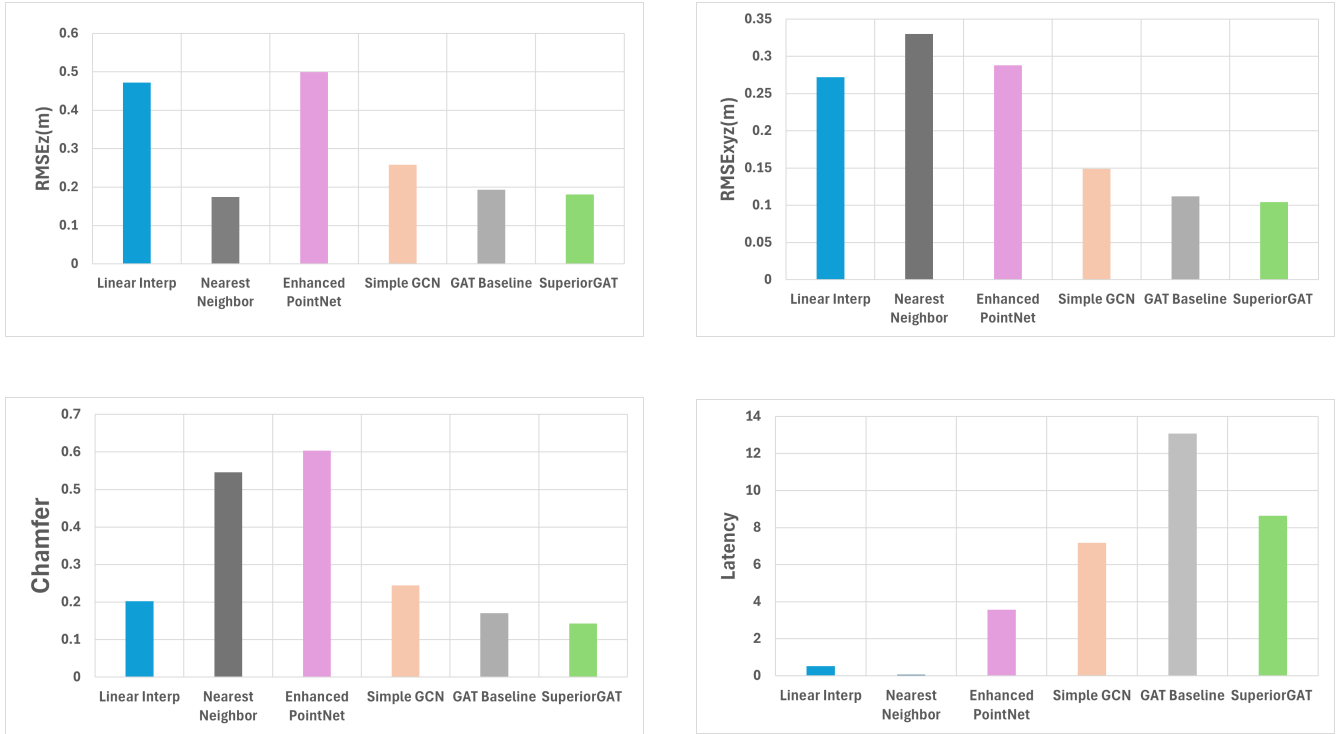


Figure 6. Comparative benchmarking of SuperiorGAT ($k = 10$) across: (a) Mean $RMSE_z$, (b) Mean $RMSE_{xyz}$, (c) Mean Chamfer Distance(m), and (d) Inference Latency(s).

shows a slightly lower vertical error ($RMSE_z = 0.174$ m compared to SuperiorGAT’s 0.181 m), this marginal gain is misleading in the context of 3D scene fidelity. NN interpolation is a purely local operator that preserves exact elevations but ignores spatial context, resulting in severe "staircase" artifacts and poor global coordinate alignment, as evidenced by its high $RMSE_{xyz}$ (0.330 m) and the second-worst Chamfer distance (0.546 m). SuperiorGAT effectively balances local vertical precision with global geometric consistency.

Regarding computational efficiency, SuperiorGAT exhibits a latency of 8.63 s, which is significantly faster than the standard GAT Baseline (13.08 s). While traditional methods, such as linear and NN interpolation, are near-instantaneous (< 1 ms), they lack the learnable parameters required to model complex terrain geometries or adapt to beam dropout patterns. The increased latency in SuperiorGAT is a necessary trade-off for the attention mechanism’s ability to dynamically weight the importance of neighbors based on spatial features. While the current graph-based implementation reflects the computational intensity of neighbor searching, the refined SuperiorGAT architecture achieves a 34% reduction in processing time compared to deeper GAT baselines. This establishes a high accuracy-to-latency ratio for graph-based point cloud recovery and provides a viable foundation for future real-time optimization on specialized hardware.

To evaluate the robustness and adaptability of the proposed model across diverse operational environments, we conducted a comprehensive cross-dataset validation using five distinct KITTI sequences: **Residential, City, Person, Campus, and Road**. These environments encompass a wide spectrum of geometric complexities, ranging from structured urban corridors to dynamic scenes featuring pedestrians and open highway surfaces.

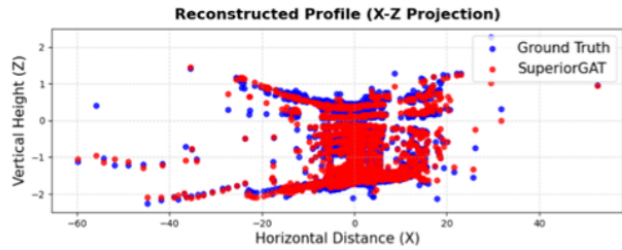
The comparative performance of SuperiorGAT against baseline and state-of-the-art methods is summarized in Table 1. The results demonstrate that SuperiorGAT consistently achieves superior reconstruction accuracy, maintaining an $RMSE_{xyz}$ of under 0.11m across all tested environments. Notably, while the Nearest Neighbor (NN) approach yields competitive $RMSE_z$ values in specific scenarios, it exhibits significantly higher Chamfer Distances—frequently exceeding double that of our model. This discrepancy indicates that NN fails to preserve the underlying structural geometry of the point cloud. In contrast, SuperiorGAT provides a balanced optimization between vertical precision and global spatial fidelity. Furthermore, our model maintains a consistent inference latency of approximately 8.6 s per frame, representing a significant computational improvement over standard multi-layer graph architectures and ensuring a high accuracy-to-latency ratio for complex spatial reconstruction.

Figure 7 presents a qualitative comparison between the original ground truth LiDAR data and the reconstructed vertical profiles generated by SuperiorGAT across the Person, Road, Campus, and City datasets. Each panel provides a camera-

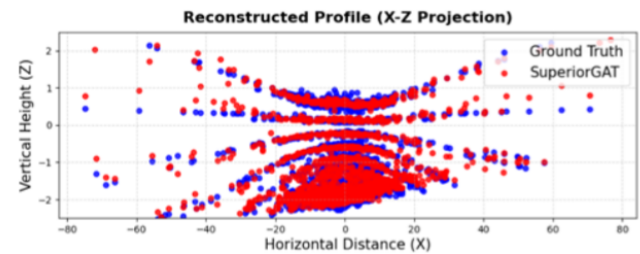
Table 1. Performance Comparison Across Different KITTI Environments (Mean \pm SD)

Dataset	Method	$RMSE_z$ (m)	$RMSE_{xyz}$ (m)	Chamfer Distance (m)	Time (s)
Residential	Linear Interp	0.472 \pm 0.102	0.272 \pm 0.059	0.202 \pm 0.015	0.51 \pm 0.02
	Nearest Neighbor	0.174 \pm 0.065	0.330 \pm 0.031	0.546 \pm 0.019	0.05 \pm 0.00
	Enhanced PointNet	0.499 \pm 0.132	0.288 \pm 0.076	0.603 \pm 0.178	3.57 \pm 0.06
	Simple GCN	0.258 \pm 0.056	0.149 \pm 0.032	0.244 \pm 0.016	7.18 \pm 0.05
	GAT Baseline	0.193 \pm 0.054	0.112 \pm 0.031	0.170 \pm 0.008	13.08 \pm 0.28
	SuperiorGAT (Ours)	0.181 \pm 0.057	0.104 \pm 0.033	0.143 \pm 0.008	8.63 \pm 0.06
City	Linear Interp	0.437 \pm 0.048	0.252 \pm 0.028	0.213 \pm 0.025	0.56 \pm 0.03
	Nearest Neighbor	0.131 \pm 0.026	0.224 \pm 0.048	0.373 \pm 0.078	0.05 \pm 0.00
	Enhanced PointNet	0.461 \pm 0.109	0.266 \pm 0.063	0.511 \pm 0.133	3.64 \pm 0.08
	Simple GCN	0.307 \pm 0.024	0.177 \pm 0.014	0.327 \pm 0.033	7.26 \pm 0.10
	GAT Baseline	0.229 \pm 0.034	0.132 \pm 0.020	0.244 \pm 0.037	13.23 \pm 0.09
	SuperiorGAT (Ours)	0.152 \pm 0.029	0.088 \pm 0.017	0.147 \pm 0.035	8.70 \pm 0.08
Person	Linear Interp	0.470 \pm 0.009	0.271 \pm 0.005	0.208 \pm 0.004	0.53 \pm 0.02
	Nearest Neighbor	0.110 \pm 0.008	0.229 \pm 0.014	0.373 \pm 0.006	0.05 \pm 0.00
	Enhanced PointNet	0.350 \pm 0.058	0.202 \pm 0.033	0.417 \pm 0.073	3.56 \pm 0.03
	Simple GCN	0.252 \pm 0.011	0.145 \pm 0.007	0.262 \pm 0.011	7.14 \pm 0.04
	GAT Baseline	0.211 \pm 0.010	0.122 \pm 0.006	0.217 \pm 0.009	13.10 \pm 0.03
	SuperiorGAT (Ours)	0.147 \pm 0.011	0.085 \pm 0.006	0.139 \pm 0.013	8.58 \pm 0.03
Campus	Linear Interp	0.412 \pm 0.041	0.238 \pm 0.024	0.217 \pm 0.015	0.52 \pm 0.02
	Nearest Neighbor	0.146 \pm 0.011	0.265 \pm 0.036	0.456 \pm 0.009	0.05 \pm 0.00
	Enhanced PointNet	0.433 \pm 0.103	0.250 \pm 0.059	0.497 \pm 0.128	3.67 \pm 0.05
	Simple GCN	0.254 \pm 0.023	0.147 \pm 0.013	0.252 \pm 0.018	7.29 \pm 0.07
	GAT Baseline	0.211 \pm 0.017	0.122 \pm 0.010	0.205 \pm 0.016	13.25 \pm 0.10
	SuperiorGAT (Ours)	0.166 \pm 0.019	0.096 \pm 0.011	0.149 \pm 0.011	8.74 \pm 0.05
Road	Linear Interp	0.470 \pm 0.009	0.271 \pm 0.005	0.208 \pm 0.004	0.52 \pm 0.01
	Nearest Neighbor	0.110 \pm 0.008	0.229 \pm 0.014	0.373 \pm 0.006	0.05 \pm 0.00
	Enhanced PointNet	0.350 \pm 0.058	0.202 \pm 0.033	0.417 \pm 0.073	3.57 \pm 0.03
	Simple GCN	0.252 \pm 0.011	0.145 \pm 0.007	0.262 \pm 0.011	7.14 \pm 0.04
	GAT Baseline	0.211 \pm 0.010	0.122 \pm 0.006	0.217 \pm 0.009	13.11 \pm 0.04
	SuperiorGAT (Ours)	0.147 \pm 0.011	0.085 \pm 0.006	0.139 \pm 0.013	8.59 \pm 0.03

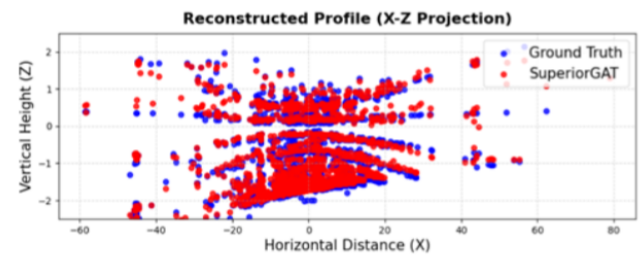
view reference (left) for operational context alongside the corresponding 2D X-Z projection (right). For visual clarity, the reconstruction is shown using a sampling stride of 15, highlighting the model’s high geometric fidelity in recovering vertical structural height (Z) based on horizontal distance (X)



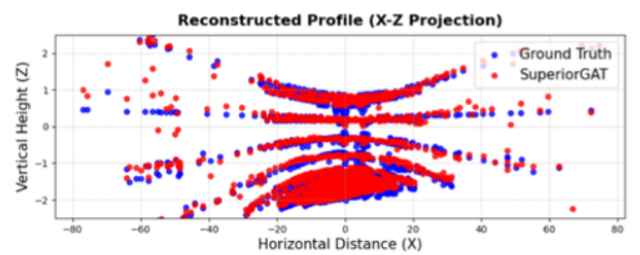
(a) Person Dataset Sample



(b) Road Dataset Sample



(c) Campus Dataset Sample



(d) City Dataset Sample

Figure 7. Qualitative reconstruction results across four datasets: (a) Person, (b) Road, (c) Campus, and (d) City. Red points (SuperiorGAT) demonstrate high vertical alignment with blue points (Ground Truth) in the X-Z projection.

Conclusion

This paper presented **SuperiorGAT**, a graph attention-based framework for reconstructing missing elevation information in sparse LiDAR point clouds under structured beam dropout. By modeling LiDAR scans as beam-aware graphs and enhancing standard graph attention networks with gated residual fusion and feed-forward refinement, the proposed approach effectively recovers lost vertical geometry while maintaining computational efficiency, without increasing network depth.

Experimental evaluations across diverse KITTI sequences, including **Person**, **Road**, **Campus**, and **City** environments, demonstrate that SuperiorGAT consistently achieves lower reconstruction error and improved geometric consistency compared to traditional interpolation methods, PointNet-based models, and deeper GAT baselines. These results indicate that targeted architectural refinement is more critical than increasing graph depth for accurate reconstruction in scenarios characterized by structured vertical sparsity.

Qualitative analyses based on X–Z projection profiles further confirm that SuperiorGAT preserves structural integrity across diverse scenes with minimal vertical distortion. Since the proposed method operates independently of temporal or RGB data and offers a significant reduction in latency compared to multi-layer graph architectures, it provides a practical and scalable framework for autonomous perception. Future work will focus on optimizing the neighbor-search mechanisms to further reduce inference time and extending the framework to dynamic dropout patterns to improve stability in highly transient environments.

References

1. Zhang, J. *et al.* Lidar degradation in adverse weather: a review for autonomous driving. *IEEE Trans. Intell. Transp. Syst.* **23**, 6100–6116 (2022).
2. Geiger, A. *et al.* Vision meets robotics: the kitti dataset. *Int. J. Robot. Res.* **32**, 1231–1237 (2013).
3. Behley, J. *et al.* Semantickitti: a dataset for lidar semantic segmentation. *Proc. IEEE Int. Conf. Comput. Vis. (ICCV)* 9297–9307 (2019).
4. Dosovitskiy, A. *et al.* Carla: an open urban driving simulator. *Conf. Robot Learn. (CoRL)* (2017).
5. Candès, E. & Tao, T. Near-optimal signal recovery from random projections: universal encoding strategies? *IEEE Trans. Inf. Theory* **52**, 5406–5425 (2006).
6. Donoho, D. Compressed sensing. *IEEE Trans. Inf. Theory* **52**, 1289–1306 (2006).
7. Wang, W. *et al.* Voxnet: end-to-end learning for point cloud based 3d object detection. *Proc. IEEE Conf. Comput. Vis. Pattern Recognit. (CVPR)* 4490–4499 (2018).
8. Hatun, H. Graph neural networks (gnns): Gcn and gat python implementation (2023).
9. Qi, C. R. *et al.* Pointnet++: deep hierarchical feature learning on point sets in a metric space. *Adv. Neural Inf. Process. Syst. (NeurIPS)* **30** (2017).
10. Scarselli, F. *et al.* The graph neural network model. *IEEE Trans. Neural Netw.* **20**, 61–80 (2009).
11. Velickovic, P. *et al.* Graph attention networks. *stat* **1050**, 10–48550 (2017).
12. Turati, A. Incorporating edge features into graph neural networks (2022).
13. Kipf, T. & Welling, M. Semi-supervised classification with graph convolutional networks. *Int. Conf. Learn. Represent. (ICLR)* (2017).
14. Awedat, K., Abidalrekab, M. & El-Yabroudi, M. A graph attention network-based framework for reconstructing missing lidar beams (2025). [2512.12410](https://doi.org/2512.12410).
15. Eskandar, G. *et al.* Hals: a height-aware lidar super-resolution framework for autonomous driving. *arXiv preprint* DOI: [10.48550/arXiv.2310.12395](https://doi.org/10.48550/arXiv.2310.12395) (2023).
16. Glennie, C. *et al.* Static calibration and analysis of the velodyne hdl-64e s2 for high accuracy mobile scanning. *Remote. Sens.* **5**, 1690–1706, DOI: [10.3390/rs5041690](https://doi.org/10.3390/rs5041690) (2013).
17. Rusu, R. B. *et al.* Fast point feature histograms for 3d registration. *IEEE Int. Conf. on Robotics Autom. (ICRA)* DOI: [10.1109/ROBOT.2009.5152771](https://doi.org/10.1109/ROBOT.2009.5152771) (2009).
18. You, J. & Kim, Y.-K. Up-sampling method for low-resolution lidar point cloud to enhance 3d object detection in an autonomous driving environment. *Sensors* **23**, 322, DOI: [10.3390/s23010322](https://doi.org/10.3390/s23010322) (2023).
19. Graham, B. *et al.* 3d semantic segmentation with submanifold sparse convolutional networks. *Proc. IEEE Conf. on Comput. Vis. Pattern Recognit. (CVPR)* DOI: [10.1109/CVPR.2018.00715](https://doi.org/10.1109/CVPR.2018.00715) (2018).

20. Wang, Y. *et al.* Dynamic graph cnn for learning on point clouds. *ACM Transactions on Graph. (TOG)* **38**, DOI: [10.1145/3306346.3322987](https://doi.org/10.1145/3306346.3322987) (2019).
21. Bahdanau, D., Cho, K. & Bengio, Y. Neural machine translation by jointly learning to align and translate. *Int. Conf. on Learn. Represent. (ICLR)* DOI: [10.48550/arXiv.1409.0473](https://doi.org/10.48550/arXiv.1409.0473) (2015).
22. Li, G., Muller, M., Thabet, A. & Ghanem, B. Deepgcns: Can gcns go as deep as cnns? In *Proceedings of the IEEE/CVF international conference on computer vision*, 9267–9276 (2019).
23. Bresson, X. & Laurent, T. Residual gated graph convnets. *arXiv preprint arXiv:1711.07553* (2017).
24. Dwivedi, V. P. & Bresson, X. A generalization of transformer networks to graphs. *arXiv preprint arXiv:2012.09699* (2020).
25. Wu, Z. *et al.* A comprehensive survey on graph neural networks. *IEEE Trans. Neural Netw. Learn. Syst.* **32**, 4–24 (2021).
26. Gilmer, J., Schoenholz, S. S., Riley, P. F., Vinyals, O. & Dahl, G. E. Neural message passing for quantum chemistry. In *Proc. 34th Int. Conf. Mach. Learn. (ICML)*, 1263–1272 (2017).
27. Wu, F. *et al.* Simplifying graph convolutional networks. In *Proc. 36th Int. Conf. Mach. Learn. (ICML)*, 6861–6871 (2019).
28. Geiger, A., Lenz, P., Stiller, C. & Urtasun, R. Vision meets robotics: The kitti dataset. *Int. J. Robotics Res. (IJRR)* (2013).